

# Reduction of nonlinear dynamic systems by phase space analysis

E. Becker

*Institut für Atmosphärenphysik an der Universität Rostock e.V., Kühlungsborn, Germany*

U. Brosa

*Brosa GmbH, Am Brücker Tor 4, D-35287 Amöneburg, Germany*

T.A. Kowalewski<sup>1</sup>

*Max-Planck-Institut für Strömungsforschung, Göttingen, Germany*

(Received March 10, 1994)

We look directly into the phase space of experimental or numerical data to derive nonlinear equations of motion. Our example is the dynamics of viscous droplets. While the smallest useful dimension of phase space turns out to be three, we apply methods to visualize four, five, six dimensions and more. These methods are Poincaré sections and condensation of variables. The resulting equations of motion are extremely simple but nevertheless realistic.

## 1. INTRODUCTION

Numerical models produce a huge amount of data but often do not facilitate a better understanding of the physical problem. Nevertheless, comprehensive numerical studies are necessary as a first step when there are no suitable approximations at hand. The indispensable second step of identifying the main physical properties and developing a simple analytical description often represents a major difficulty.

Usually, data sets are evaluated by plotting time series, Fourier spectra, various statistical properties etc. But nonlinearities depreciate these techniques as they rarely yield concise and thus instructive descriptions.

The aim of this paper is to show that the concept of phase space in connection with interactive computer graphics [1] can be used to perform the second step even if nonlinearities prevail. Instead of a formal description we discuss an actual example: nonlinear oscillations of a viscous droplet.

The dynamics of a droplet formed by an incompressible viscous fluid is one of the classical problems in hydrodynamics which has occupied many scientists during the last two centuries. The only analytical accounts for this subject are the linear theory of small amplitude oscillations [2-4] and the weakly nonlinear approximations of Tsamopoulos and Brown [5] and Natarajan and Brown [6] for strictly periodic solutions. On the other hand, measurements and numerical investigations show that these analytical approaches agree poorly with reality [7,8]. Even the asymptotic dynamics of small amplitude oscillations seems to be dominated by nonlinearities, leading to phenomena like self-organisation of the surface modes [9], in contradiction to the analytical theories. However, further measurements and numerical computations do not help in understanding these discrepancies.

---

<sup>1</sup>On leave of absence from the Institute of Fundamental Technological Research, Polish Academy of Sciences, Warsaw, Poland

After giving a brief summary of available droplet models and experimental results (Sections 2 and 3), an appropriate system of simple differential equations is developed in Section 4. This system, when compared with the full models, drastically reduces the computation time and the required size of computer memory. The fact – mysterious at first sight – that nonlinear effects dominate even for very small oscillation amplitudes becomes evident. Moreover, the reduced equations are essential for practical applications like surface tension measurement.

## 2. MODELLING NONLINEAR DROPLET DYNAMICS

The mathematical description of axisymmetric droplet oscillations is based on the surface parametrization (see Fig. 1)

$$R(\theta, t) = r_0 \left\{ a_0(a_2 \dots a_{l_0}) + \sum_{l=2}^{l_0} a_l(t) P_l(\cos \theta) \right\}. \tag{1}$$

The droplet radius  $R$  in spherical coordinates  $(r, \theta)$  is expanded as a series of Legendre polynomials. The free parameters  $a_2 \dots a_{l_0}$  are time-dependent amplitudes of standing surface waves. The fundamental mode  $a_2$  describes elongation and contraction, i.e. prolate and oblate droplet forms. Each surface wave  $a_l$  consists of  $l$  wavelengths encircling the cross-section of the droplet.  $a_0$  is a function of the surface parameters  $a_2 \dots a_{l_0}$  to ensure the conservation of the droplet volume  $\frac{4}{3}\pi r_0^3$ .  $a_1$  is neglected because it represents only translational motion. The parametrization (1) has been used by Becker et al. [9,10] for experimental and theoretical analysis.

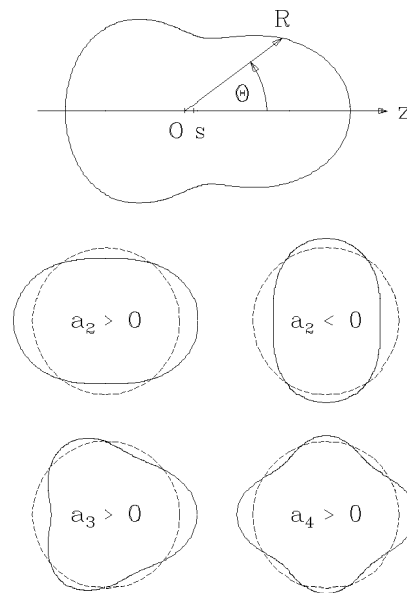


Fig. 1. A droplet cross-section described by the surface parametrization (1) in spherical coordinates  $(r, \theta)$ .  $s$  denotes the centre of mass with respect to the origin  $O$ . Deformations due to the first three surface waves (solid lines) compared with the equivolumetric sphere (dashed lines) are displayed below at a smaller scale

To our knowledge, only two droplet models which take into account all nonlinear and viscous effects are available up to now. The first, given by Basaran [8], is based on the Galerkin/finite-element technique. The second, by Becker et al. [9], starts out with appropriate mode expansions for the droplet surface (Eq. (1)) and the velocity field. These mode expansions follow from linear analysis [4]. A system of ordinary differential equations for the mode amplitudes is derived by the Gaussian variational principle.

Alternatively, one can describe the dynamics of a viscous droplet with the approximation of vanishing vorticity. This is possible because in the case of free boundary conditions the vorticity of the surface layer remains finite while its thickness goes to zero with increasing Reynolds number. Lamb [3] made use of this fact in his calculation of the linear damping constants. Fortunately, the study of our experimental results (performed with ethanol and water droplets of approximately 0.5 mm in diameter) has recently shown that the irrotational approximation is also appropriate for the interpretation of large amplitude oscillations.

The possibility of applying Lamb's method to the nonlinear equations has been demonstrated by Lundgren and Mansour [7]. Using the boundary-integral method, their resulting numerical procedure remains tedious and time consuming, hence difficult to be implemented for practical applications. Another way is offered by the formalism of classical mechanics, describing droplet dynamics in terms of effective masses, kinetic and surface energy, and a dissipation tensor. The advantage over pure numerics is twofold: first, the numerical evaluation of the governing equations is straightforward and requires only standard methods and second, the whole dynamics is determined by a few degrees of freedom, i.e. the generalized coordinates  $a_2 \dots a_{l_0}$  and their velocities  $\dot{a}_2 \dots \dot{a}_{l_0}$ . A corresponding model for nonlinear droplet oscillations is given in the appendix.

Further simplification of modelling nonlinear droplet dynamics is possible by neglecting all viscous terms. This approach is realistic only for time scales shorter than approximately one oscillation period of  $a_2$  (e.g. droplet fission [11]). As we will see in Section 4, the long-time behaviour of an oscillating droplet cannot in any way be described without the impact of viscosity.

### 3. TIME SERIES OF OBSERVED DROPLET OSCILLATIONS

In the following we discuss typical experimental results compared with the predictions of the full nonlinear and viscous model (M1) given in [9], the nonlinear, irrotational (but still viscous) model described in the appendix (M2), and the linear Lamb [3] model (M3), defined by Eqs. (24) and (25).

Fig. 2 shows the first four surface modes  $a_2 \dots a_5$  as functions of time for small ethanol droplets. Observed data are compared with the predictions of M1 and M2 in Fig. 2a. These computations require initial values for the surface amplitudes  $a_l$  and their velocities  $\dot{a}_l$  as well as the knowledge of the fluid density  $\rho$ , the kinematic viscosity  $\nu$ , the surface tension  $\sigma$  and the equivolumetric radius  $r_0$ . The time unit defined by

$$T_0 = \sqrt{\rho r_0^3 / 3\sigma} \quad (2)$$

is about  $\frac{1}{4}ms$  for the experimental conditions of Fig. 2. The value of the Reynolds number, defined as

$$Re = \frac{r_0^2/T_0}{\nu}, \quad (3)$$

determines whether the irrotational approximation is appropriate or not. In the case of small ethanol droplets ( $Re \approx 90$ ) the nonlinear models M1 and M2 seem to be equivalent for the description of measurements.

The time series in Figs. 2a,b are typical for most of our measurements and, as we will see, represent the general asymptotic dynamics. A qualitative characterization follows from the comparison of nonlinear and linear results (Fig. 2b).

First of all we notice the well-known enlargement of the oscillation period of  $a_2$ . In detail the frequency of  $a_2$  decreases during the droplet's elongation ( $a_2 > 0$ ) but increases during its contraction ( $a_2 < 0$ ), in other words: a self-generated frequency modulation. A similar modulation effect is carried out in the time evolution of  $a_3$ . It oscillates more slowly during positive displacements of  $a_2$  and faster during negative ones. Hence the frequency of  $a_3$  is modulated by  $a_2$ . Qualitatively,  $a_2$  and  $a_3$  exhibit damped harmonic oscillations, and the nonlinear modulation effects disappear for  $t \rightarrow \infty$ .

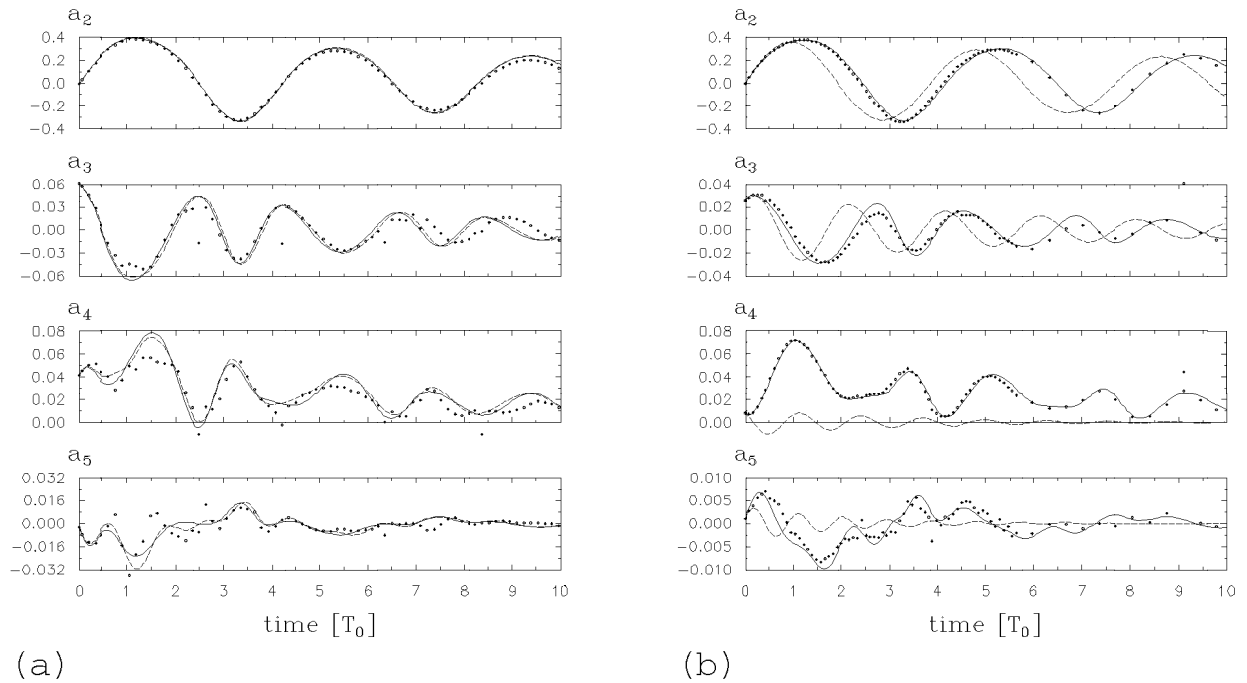


Fig. 2. Time series of observed droplet oscillations. (a) Experimental data (dotted lines) and computational results (M1: solid lines, M2: dashed lines); an ethanol droplet with  $r_0 = 0.1733$  mm and  $Re = 81$  (see Fig. 13 in ref. [9]). (b) Experimental data (dotted lines), nonlinear simulation with M2 (solid lines), linear theory M3 (dashed lines); an ethanol droplet with  $r_0 = 0.207$  mm and  $Re = 89$  (see Fig. 9 in ref. [9])

On the other hand, for the higher modes  $a_4$  and  $a_5$  the differences between nonlinear and linear results are qualitative. For example,  $a_4$  remains almost always positive. It is phase locked with  $a_2$  and oscillates with double its frequency. According to linear theory (25) a trebling of the fundamental frequency would be expected. Moreover, these nonlinear effects should disappear asymptotically. As already mentioned in Section 1, this is not the case.

The differences between linear and asymptotic dynamics are also illustrated by the computation shown in Fig. 3 where artificial initial conditions have been used. The oscillation starts with strongly excited modes  $a_4$  and  $a_5$ . The modes  $a_2$ ,  $a_3$  and  $a_6$  get weakly excited due only to nonlinear couplings and are not shown. It is very important to note that the energy carriers  $a_4$  and  $a_5$  can initially be described very well by the linear model M3, although their amplitudes exceed those present in “natural” oscillations. But what happens at  $t \rightarrow \infty$ ? Fig. 3 shows time intervals after several periods of the fundamental mode. For  $t/T_0 = 50 \dots 60$  the linear theory yields drastic deviations from the nonlinear simulation. Later on, the asymptotic dynamics has fully developed, and the time series, although at invisible small amplitudes, look similar to those shown in Fig. 2. The aim is to understand these unexpected effects by a realistic, nevertheless extremely simplified theory.

#### 4. THE REDUCED DIFFERENTIAL EQUATIONS

We are looking for ordinary differential equations of the form

$$LD_l + \dots = 0, \quad l = 2 \dots 5 \quad (4)$$

where  $LD_l$  represents the nondimensional linear terms

$$LD_l = b_l + \frac{l(l+2)(l-1)}{3} a_l + 2 \frac{(2l+1)(l-1)}{Re} v_l \quad v_l = \dot{a}_l T_0, \quad b_l = \ddot{a}_l T_0^2 \quad (5)$$

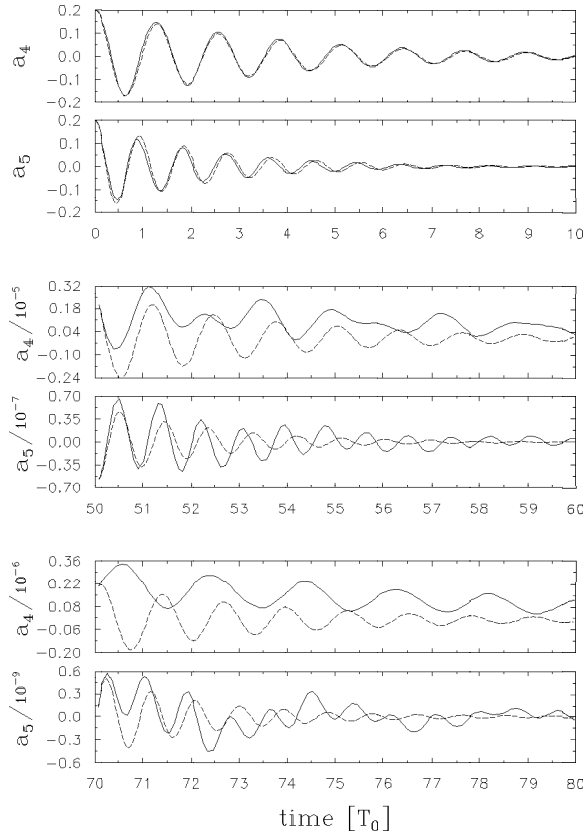


Fig. 3. Comparison of nonlinear (M2, solid lines) and linear (M3, dashed lines) description for artificial initial conditions with excited modes  $a_4(0) = a_5(0) = 0.2$  only. Three time intervals are displayed, monitoring the initial behaviour, the transition regime and the asymptotic behaviour. The Reynolds number is 100

and the unknown effective nonlinear terms are indicated by the ellipsis in (4).

The amplitudes  $a_2 \dots a_5$ , their nondimensional velocities  $v_2 \dots v_5$  and accelerations  $b_2 \dots b_5$  generate a 12-dimensional phase space. In order to derive the effective nonlinearities we have to “fly” through that space and analyse the surfaces

$$f(a_2 \dots a_5, v_2 \dots v_5, b_2 \dots b_5) = 0 \quad (6)$$

that are formed by an assembly of trajectories. These surfaces are already defined by the full, yet noninstructive differential Eqs. (21). We ask whether they can be approximated by simple algebraic expressions.

The numerical integration of the full differential equations yields the vector  $(a_2 \dots a_5, v_2 \dots v_5, b_2 \dots b_5)$  as a discrete function of time. In the following we inspect an assembly of trajectories generated with the irrotational droplet model M2. The initial conditions correspond to measurements with maximum droplet deformations of about 50% (with respect to equivolumetric radius  $r_0$ ) and  $Re \approx 90$ .

Let us start with the subspace  $a_2, v_2, b_2$  of the fundamental mode (Fig. 4a). If  $a_2$  was a linear oscillator ( $LD_2 = 0$ ), we would observe a plane. The nonlinear computations yield a saddle. This result contains all information about the effective differential equation. From the fact that a surface is visible in the  $a_2, v_2, b_2$ -projection, we can conclude that  $a_2$  is ruled by itself and is not affected by other modes. The special form of a saddle requires that the effective nonlinearities are proportional to  $a_2^2$  and  $v_2^2$ . Hence, the reduced differential equation may be written

$$b_2 + \frac{8}{3}(1 - [1.36 \pm 0.04]a_2)a_2 + \frac{10}{Re}v_2 - [0.6 \pm 0.1]v_2^2 = 0, \quad (7)$$

where the bold numbers in brackets follow from fitting  $LD_2 + \frac{8}{3}[\ ] \cdot a_2^2 + [\ ] \cdot v_2^2 = 0$  to the data. The values of the standard deviations measure the significance of the coefficients. Notice that the frequency modulation  $\frac{8}{3} 1.36 a_2$  is of order unity, i.e. it is as important as the term known from linear analysis  $\frac{8}{3}$ .

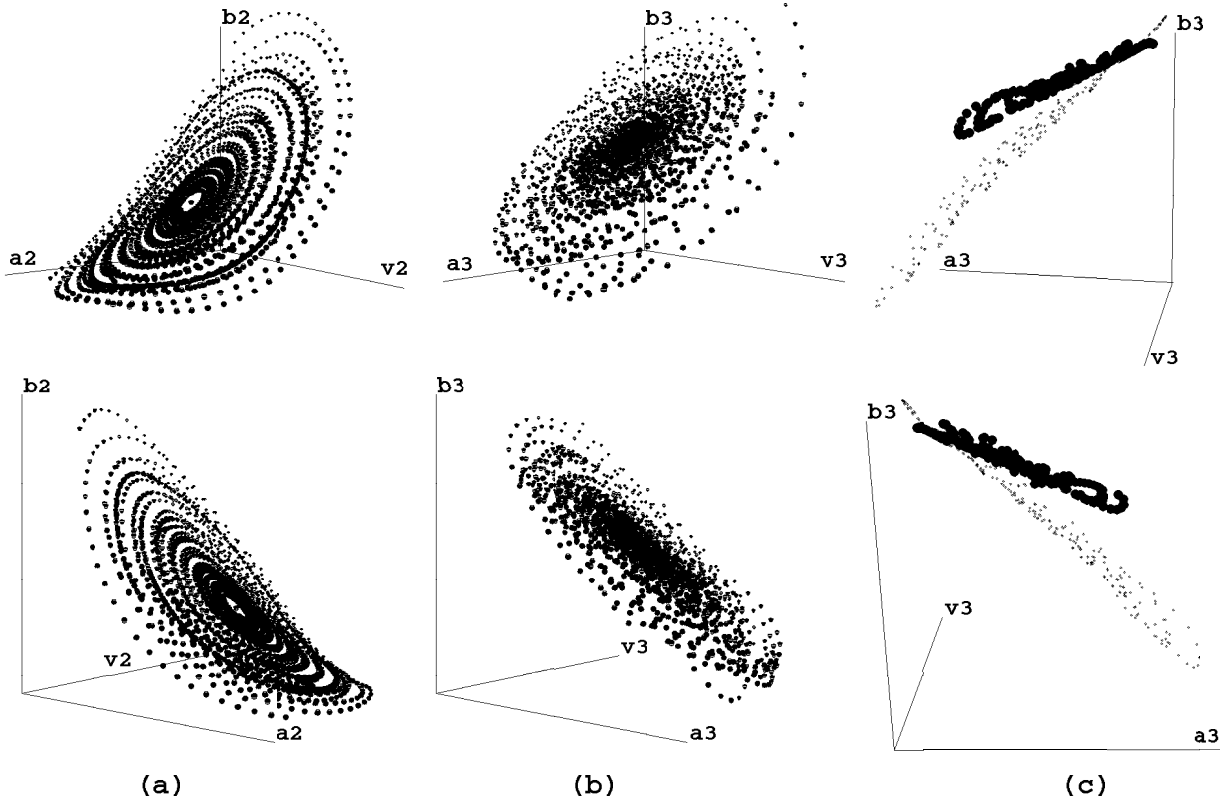


Fig. 4. Phase space views. (a) and (b) — the subspaces  $(a_2, v_2, b_2)$  and  $(a_3, v_3, b_3)$ , respectively. The size of the data points corresponds to their position with respect to the picture plane. (c) — two Poincaré sections with respect to  $a_2$ . The size of the data points corresponds to  $a_2$

Examination of fig. 4b shows that in the  $a_3, v_3, b_3$  subspace the points do not form a surface. We observe an irregular change of their depth (marked here by point size) in the figure plane. Hence,  $a_3$  is influenced by other modes, and the surface defined by  $LD_3 + \dots = 0$  lies within at least a four-dimensional subspace. We can analyze this surface using the method of Poincaré.

From the discussion in the previous section we conclude that  $b_3$  is a function of  $a_3, v_3$  and  $a_2$ . This can be proved by considering Poincaré sections with fixed  $a_2$ . Therefore we generate several data subsets, each containing only phase space points with  $a_2$  confined within a certain interval. In Fig. 4c two of these Poincaré sections are shown in the  $a_3, v_3, b_3$ -projection. The heavy and light points correspond to the largest and smallest values of  $a_2$ , respectively. Each Poincaré section forms approximately a plane whose slope with respect to  $a_3$  obviously depends on the size of points, i.e. on the value of  $a_2$ . This behaviour allows the evaluation of coefficients in the assumed form of the differential equation, i.e.  $b_3 = f_1(a_2) a_3 + f_2 v_3$ . Determining the slope of every Poincaré section  $a_2 \approx const$ ,  $f_1$  turns out to be approximately a linear function of  $a_2$ ,  $f_1 \approx f_1(0) + f_1'(0) a_2$ . Comparing this result with (5) and fitting  $f_1'(0)$  to the data, we obtain

$$b_3 + 10(1 - [1.53 \pm 0.09] a_2) a_3 + \frac{28}{Re} v_3 = 0. \quad (8)$$

In contrast to (7) no term proportional to  $v_3^2$  occurs, which agrees with parity.

The time series of  $a_4$  and  $a_5$  (Figs. 2 and 3) suggest that these modes are driven by the energy carriers  $a_2$  and  $a_3$ . Because of parity we expect  $a_2^2$  and  $v_2^2$  as driving terms for  $a_4$  or  $a_2a_3$  and  $v_2v_3$  for  $a_5$ . Furthermore, there must be terms to facilitate frequency modulation, namely  $a_2a_4$  or  $a_3a_5$ . We inspected, therefore, the phase spaces  $(LD_4, a_2^2, v_2^2, a_2a_4)$  or  $(LD_5, a_2a_3, v_2v_3, a_2a_5)$  that take 5 or even 7 variables into account. Fixing  $a_2a_4$  or  $a_2a_5$ , all three-dimensional Poincaré sections showed up as planes. Hence the same procedures as described above can be applied. They yield differential equations for  $a_4$  and  $a_5$ :

$$b_4 + 24(1 - [\mathbf{0.35} \pm \mathbf{0.07}]a_2)a_4 + \frac{54}{Re}v_4 = [\mathbf{8.32} \pm \mathbf{0.08}]a_2^2 + [\mathbf{1.54} \pm \mathbf{0.06}]v_2^2 \quad (9)$$

$$b_5 + \frac{140}{3}(1 - [\mathbf{0.4} \pm \mathbf{0.2}]a_2)a_5 + \frac{88}{Re}v_5 = [\mathbf{32.1} \pm \mathbf{1.3}]a_2a_3 + [\mathbf{3.7} \pm \mathbf{0.1}]v_2v_3. \quad (10)$$

Eqs. (9) and (10) make clear to us why linear theory fails to describe the small amplitude oscillations of the full mode system. We can see that the damping constants  $(2l+1)(l-1)/Re$  become large for the higher modes. Hence, after a few oscillation periods the influence of the initial conditions diminishes for  $a_4$  and  $a_5$  and these modes reflect the driving forces from  $a_2$  and  $a_3$ . In the case of  $a_4$  this force is always positive and oscillates with twice the frequency of  $a_2$ . Summarizing: linear damping selects certain nonlinearities that asymptotically dominate the linear terms. Such a mode locking mechanism has already been described by Haken [12].

Obviously, the empirically derived second order terms can also be calculated by a Taylor series expansion of mass tensor and surface energy in (21). If we assume the effective nonlinearities to consist of all second order terms that follow from the Taylor expansion, we receive numerous terms in each differential equation. We have checked a few of our results by those tedious calculations (Table 1). The accuracy of the effective terms is satisfactory as they incorporate the influence of many nonlinearities.

Table 1. The empirically determined coefficients of the non-linear terms in Eqs. (7) and (8) compared with the corresponding Taylor coefficients

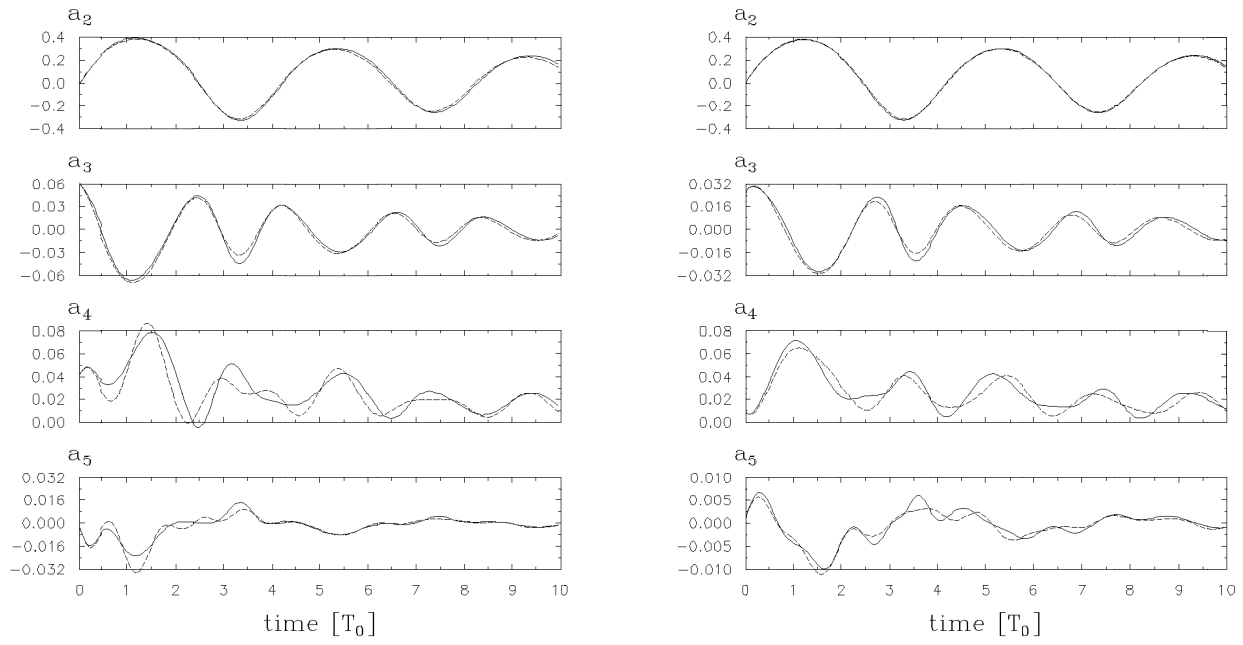
nonlinearity	empirical coefficient	Taylor coefficient
$-a_2^2$	$\frac{8}{3}[\mathbf{1.36} \pm \mathbf{0.04}]$	$\frac{8}{3}[\mathbf{1.43}]$
$-v_2^2$	$[\mathbf{0.6} \pm \mathbf{0.1}]$	$[\mathbf{0.643}]$
$-a_2a_3$	$10[\mathbf{1.53} \pm \mathbf{0.09}]$	$10[\mathbf{1.64}]$

Finally let us test the differential Eqs. (7)–(10) by considering familiar time series once again. Figs. 5a and b show results of Fig. 2 compared with the predictions of the reduced model. The modes  $a_2$  and  $a_3$  agree quite well,  $a_4$  and  $a_5$  at least qualitatively. In the case of smaller initial amplitudes (Fig. 5c) all surface modes are in good agreement.

## 5. CONCLUDING REMARKS

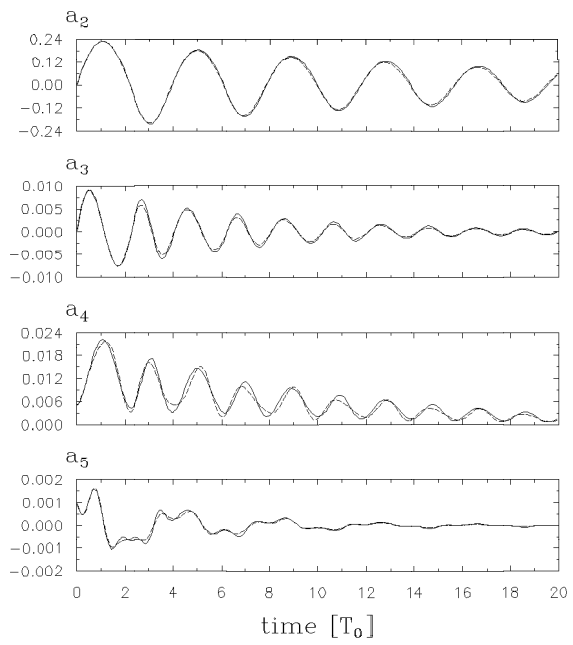
The proposed method of reducing nonlinear dynamic systems consists of a “flight” through a high dimensional phase space. One needs to take advantage of software packages for interactive graphical data manipulation.

The system of ordinary differential Eqs. (7)–(10) describes quantitatively the asymptotic behaviour of nonlinear droplet oscillations. If “natural” initial conditions are chosen, the asymptotic dynamics is already reached in the domain of large amplitudes. Therefore the reduced model can be used to improve the asymptotic method [13] previously used to measure surface tension with the oscillating droplet method. Once  $\rho$ ,  $r_0$  and  $a_2(t) \dots a_5(t)$  are known from experiment, it becomes



(a)

(b)



(c)

Fig. 5. Comparisons of the reduced model (dashed lines) with the full models M1 or M2 (solid lines). (a) Initial conditions due to Fig. 2a, compared with model M1. (b) Initial conditions due to Fig. 2b, compared with model M2. (c) Initial conditions corresponding to the third time interval of Fig. 11 in [9], compared with model M1



possible to perform several calculations by modifying the time scale  $T_0$  (which means varying the initial velocities  $v_i$ ) and the Reynolds number  $Re$ . Then, least error optimization determines  $T_0$  and  $Re$ , i.e.  $\sigma$  and  $\nu$  (see definitions (2) and (3)). In principle such a procedure is also possible using the full models M1 and M2 or those of Lundgren and Mansour [7] and Basaran [8]. However, due to the huge CPU time required it is impractical. On the other hand, the reduced differential Eqs. (7)–(10) can be implemented easily on a small computer, allowing real-time evaluations of surface tension and viscosity. Moreover, the physical interpretation of the asymptotic dynamics in terms of frequency modulation and self-organisation becomes evident.

## APPENDIX

We limit our interest to axisymmetric oscillations of a viscous droplet described in spherical coordinates  $(r, \theta)$ . As a first step the droplet surface is parametrized by (1). Assuming zero vorticity inside the droplet, the velocity field can be represented by a series of velocity potentials

$$\vec{v} = -\nabla \sum_{l=2}^{l_0} \Phi_l(r, \theta; a_2 \dots a_{l_0}) \dot{a}_l, \quad \Delta \Phi_l = 0, \quad (11)$$

where in turn each potential  $\Phi_l$  is expanded as a series of partial solutions of the Laplace equation

$$\Phi_l = \sum_{i=1}^{i_{max}} c_{li}(a_2 \dots a_{l_0}) r^i P_i(\cos \theta). \quad (12)$$

The coefficients  $c_{li}$  are determined by fitting the kinematic boundary condition (see Becker et al. (1991, eq.(20))

$$\frac{d}{dt}(R(\theta, t) - r) = 0. \quad (13)$$

Using (11), the kinetic energy of the droplet can be written as a quadratic form in the generalized velocities  $\dot{a}_2 \dots \dot{a}_{l_0}$ :

$$T = \frac{1}{2} \sum_{l,m=2}^{l_0} M_{lm}(a_2 \dots a_{l_0}) \dot{a}_l \dot{a}_m. \quad (14)$$

The mass tensor  $M_{lm}$  depends only on the generalized coordinates  $a_2 \dots a_{l_0}$  and is given by

$$M_{lm} = \frac{\rho}{2} \int_{surface} (\Phi_l \nabla \Phi_m + \Phi_m \nabla \Phi_l) dS \quad (15)$$

where  $\rho$  denotes the density of the fluid. The potential energy is given by the surface tension  $\sigma$  multiplied by the area of the droplet surface:

$$V = \sigma \int_{surface} dS. \quad (16)$$

The dissipation rate of the total energy is generally given by

$$\frac{d}{dt}(T + V) = -2\rho\nu \int_{surface} \{(\vec{v} \cdot \nabla) \vec{v}\} \cdot d\vec{f} - \rho\nu \int_{volume} (\nabla \times \vec{v})^2 d\tau. \quad (17)$$

In the approximation of zero vorticity the second integral of (17) vanishes and the first can be rewritten with the use of (11) in analogy to the kinetic energy

$$\frac{d}{dt}(T + V) = -\frac{\nu}{2} \sum_{l,m=2}^{l_0} Q_{lm}(a_2 \dots a_{l_0}) \dot{a}_l \dot{a}_m \quad (18)$$

with the dissipation tensor given by

$$Q_{lm} = 2\rho \int_{\text{surface}} \{(\nabla \Phi_l \cdot \nabla) \nabla \Phi_m + (\nabla \Phi_m \cdot \nabla) \nabla \Phi_l\} dS. \quad (19)$$

The equations of motion follow from the Lagrange equations of the second kind

$$\frac{d}{dt} \frac{\partial(T - V)}{\partial \dot{a}_l} - \frac{\partial(T - V)}{\partial a_l} = \frac{1}{2} \frac{\partial}{\partial \dot{a}_l} \frac{d(T + V)}{dt}, \quad l = 2 \dots l_0, \quad (20)$$

yielding

$$\sum_{m=2}^{l_0} M_{lm} \ddot{a}_m = \sum_{n,m=2}^{l_0} \left( \frac{1}{2} \frac{\partial M_{nm}}{\partial a_l} - \frac{\partial M_{ml}}{\partial a_n} \right) \dot{a}_n \dot{a}_m - \frac{\partial V}{\partial a_l} - \frac{\nu}{2} \sum_{m=2}^{l_0} Q_{lm} \dot{a}_m, \quad l = 2 \dots l_0. \quad (21)$$

In the coordinate system defined by (1) the centre of mass is not at rest. Its deviation from the origin  $O$  along the symmetry axis is given by

$$s(a_2 \dots a_{l_0}) = \frac{3}{8} r_0 \int_{-1}^1 \cos \theta \{a_0(a_2, \dots, a_{l_0}) + \sum_{l=2}^{l_0} a_l P_l(\cos \theta)\}^4 d \cos \theta. \quad (22)$$

Thus, after evaluating the kinematic boundary condition, each velocity potential  $\Phi_l$  must be completed by

$$\Phi_l \rightarrow \Phi_l + \frac{\partial s}{\partial a_l} r \cos \theta \quad (23)$$

before the integrals (15) and (19) are computed.

It can be shown that linearization of (21) leads to the set of simple differential equations

$$\ddot{a}_l + \omega_l^2 a_l + 2 \delta_l \dot{a}_l = 0, \quad l = 2 \dots l_0 \quad (24)$$

with the frequencies and damping constants

$$\omega_l^2 = \frac{\sigma}{\rho r_0^3} l(l-1)(l+2), \quad \delta_l = \frac{\nu}{r_0^2} (2l+1)(l-1), \quad (25)$$

well known from the analysis of Rayleigh [2] and Lamb [3].

The equation system (21) can easily be solved numerically by standard methods. The computational results presented in Sections 3 and 4 were generated with  $l_0 = 6$  and  $i_{max} = 8$ .

## REFERENCES

- [1] V. Wilkening. Betrachtungen im Hyperraum — ‘Relation’ verarbeitet Multiparameter-Daten (Hyperspace investigation — ‘Relation’ handles multiparameter data). *c’t*, Heft 1:70–74, 1992
- [2] J.W.S. Rayleigh. On the capillary phenomena of jets. *Proc. R. Soc. Lond.*, **29**:71–97, 1879.
- [3] H. Lamb. *Hydrodynamics*. 6th ed., pp. 473–475 and 639–641. Cambridge University Press, 1932.
- [4] S. Chandrasekhar. *Hydrodynamic and Hydromagnetic Stability*. pp. 466–477. Oxford, Clarendon Press, 1961.
- [5] J.A. Tsamopoulos and R.A. Brown. Nonlinear oscillations of inviscid drops and bubbles. *J. Fluid Mech.*, **127**:519–537, 1983.

- 
- [6] R. Natarajan and R.A. Brown. Third-order resonance effect and the nonlinear stability of drop oscillation. *J. Fluid Mech.*, **183**:95–121, 1987.
- [7] T.S. Lundgren and N.N. Mansour. Oscillation of drops in zero gravity with weak viscous effects. *J. Fluid Mech.*, **194**:479–510, 1988.
- [8] O.A. Basaran. Nonlinear oscillations of viscous liquid drops, *J. Fluid Mech.*, **241**:169–198, 1992.
- [9] E. Becker, W.J. Hiller and T.A. Kowalewski. Nonlinear dynamics of viscous droplets. *J. Fluid Mech.*, **258**:191–216, 1994.
- [10] E. Becker, W.J. Hiller and T.A. Kowalewski. Experimental and theoretical investigation of large amplitude oscillations of liquid droplets. *J. Fluid Mech.*, **231**:189–210, 1991.
- [11] U. Brosa, S. Grossmann, A. Müller and E. Becker. Nuclear scission. *Nuclear Phys.*, **A502**:423c–442c, 1989.
- [12] H. Haken. *Synergetik*. 3d ed., pp.211-217 . Berlin, Springer-Verlag, 1990.
- [13] B. Stückrad, W.J. Hiller and T.A. Kowalewski. Measurement of dynamic surface tension by the oscillating droplet method. *Exp. in Fluids*, **15**:332–340, 1993.